DOI: 10.1039/c3ta12970e

Highly photoactive anatase nanoparticles obtained using trifluoroacetic acid as an electron scavenger and morphological control agent†

David G. Calatayud,*[a] Teresa Jardiel,[a] Marco Peiteado,[b] Cristina Fernández Rodríguez,[c] M. Rocio Espino Estévez,[c] Jose M. Doña Rodríguez,[c] Francisco J. Palomares,[d] Fausto Rubio,[a] Daniel Fernández-Hevia[ce] and Amador C. Caballero[a]

Fluorine species adsorbed on the surface of TiO_2 anatase nanoparticles improve their photocatalytic performance by reducing the recombination rate of photogenerated electrons and holes. Trifluoroacetic acid (TFAA) has been recently proposed as a promising harmless substitute for hydrofluoric acid (HF) in preparing fluorine-modified anatase with good scavenger properties. However the photocatalytic performance of the TiO_2 nanoparticles also depends on their specific morphology, by which the number and type of crystal facets, which remain exposed, are determined. A comprehensive study is presented in this contribution which for the first time describes the role of TFAA in stabilizing the highly photoactive {001} TiO_2 facets. Furthermore, by reducing the amount of water incorporated into the reaction medium, a simple one-step synthesis method is also proposed that allows the preparation of TFAA-modified anatase nanoparticles with specific morphology and selected stabilized facets, eventually yielding a semiconductor material with excellent photocatalytic properties.

Introduction

Semiconductor photocatalysts have long been studied due to their potential application in a wide range of fields such as removal of toxic pollutants and photocatalytic water decomposition. Titanium dioxide is the most widely used photocatalyst because of its exceptional optical and electronic properties, high efficiency, high photo-stability, strong oxidizing power, non-toxicity, chemical stability, and low cost.[1–4] Among the three common polymorphs of TiO_2 it is generally accepted that anatase is the most active photocatalyst.[5–11] The properties influencing the photoactivity of anatase particles have been reported to include surface area, crystallinity, crystallite size and crystal structure;[12,13] but also the morphology of the particles, by determining which crystal facets are exposed, has a strong influence on the photocatalytic performance of anatase. Although this fact is still under debate, both theoretical and experimental studies have shown that the (001) surface of anatase TiO_2 with 100% Ti five-fold coordinated (Ti_{5c}) is much more reactive than the thermodynamically more stable {101} facets with 50% Ti_{5c} and 50% Ti_{6c}.[14–18] Unfortunately {001} facets are energetically unfavorable, so their progress during crystal growth is typically constrained. However this scenario may be overcome by adapting the preparation methodology *i.e.* by suitably tuning the experimental conditions used for the synthesis, anatase nanoparticles with controlled size distribution and specific morphology can be obtained. In general the formation and growth of TiO_2 nanoparticles starts with hydrolysis and condensation processes from different Ti-precursors;[19] parameters such as the hydrolysis ratio and the nature of the precursors (alkoxides typically) are key factors for determining the kinetics of those processes. In addition surface modifications can be introduced to tailor the morphology of anatase particles. Particularly surfactants with different functional groups and distinct binding strengths might be used to control the morphology of the resulting particles. For example, the use of compounds with carboxylic groups[20] or certain fluorine-based compounds[14,21–24] has shown to be effective to stabilize the TiO_2 {001} facets. In particular fluorine atoms adsorbed on the surface of TiO_2 particles also act as good electron scavengers

[a]*Instituto de Cerámica y Vidrio, CSIC, c/Kelsen 5, Campus de Cantoblanco, 28049 Madrid, Spain. E-mail: dgcalatayud@icv.csic.es; Fax: +34 917355843; Tel: +34 917355840 ext. 1184*

[b]*POEMMA-CEMDATIC, ETSI Telecomunicación, (UPM), Av. Complutense 30, 28040 Madrid, Spain*

[c]*Group of Photocatalysis and Spectroscopy Applied to the Environment (FEAM), Department of Chemistry, Universidad de Las Palmas de Gran Canaria, Campus de Tafira, E-35017 Gran Canaria, Spain*

[d]*Department of Nanostructures and Surfaces, Instituto de Ciencia de Materiales de Madrid, CSIC, c/Sor Juana Ines de la Cruz 3, Campus de Cantoblanco, 28049 Madrid, Spain*

[e]*INAEL Electrical Systems, S.A. c/Jarama 5, 45007 Toledo, Spain*

† Electronic supplementary information (ESI) available. See DOI: 10.1039/c3ta12970e

and contribute to reduction of the recombination rate of photogenerated electrons and holes of TiO_2, so they are good candidates as well to obtain an improved photoactivity.[25] Following this line several studies have been recently reported in which fluorine atoms are used in the controlled synthesis of photoactive anatase and, in most cases, they are incorporated into the reaction system as hydrofluoric acid (HF);[14,24,26] being a strong acid, HF is a handy fluorine source and shows one additional advantage: no unwanted counter-anions are released into the medium. The problem is that HF is toxic, highly corrosive and reactive, so its use in a large-scale synthesis of faceted TiO_2 nanoparticles is categorically hindered. In this case, one less toxic and corrosive alternative to HF which has been lately considered is trifluoroacetic acid (TFAA).[27] TFAA can act as a fluorine source, capping agent, and as an acid catalyst, it can also promote the hydrolysis and inhibit the condensation reactions.[28] Like HF, TFAA has shown to be a good electron scavenger too, mainly due to the strong electron withdrawing role of the $-CF_3$ group.[29] So it seems that TFAA is a promising candidate to substitute HF in the preparation of anatase nanoparticles with enhanced photocatalytic activity. However, to the best of our knowledge there is one important feature regarding the possibilities of TFAA which has not been explored yet: its contribution to the stabilization of the {001} photoactive TiO_2 facets. Accordingly, in this research we scrutinize the role of TFAA as both a scavenger and a morphological control agent for obtaining well-faceted anatase nanoparticles. Moreover, since the use of TFAA extraordinarily reduces the presence of water incorporated into the reaction medium (in the best case HF solutions are 48% wt in water), rapid precipitation can be prevented so a better control over the hydrolysis reactions can be expected. Thus, considering the slow formation of the TFAA-modified crystallization nuclei, we have also developed a one-step semi-solvothermal route for easy preparation of anatase nanoparticles with specific morphology and selected stabilized facets.

Experimental section

Synthesis of TFAA-modified anatase TiO_2 nanoparticles (Ti-TFAA)

Well-faceted nanoparticles of TiO_2 have been synthesized through a one-step semi-solvothermal route using as received titanium(IV) tetrabutoxide ($Ti(OBut)_4$, Fluka, 98%) and trifluoroacetic acid (CF_3COOH, Aldrich, 70%, TFAA). Compared with other alkyl precursors, the butoxide group of $Ti(OBut)_4$ exhibits a slower rate of hydrolysis, thereby allowing an enhanced control of the diffusion and polymerization processes.[30,31] In a typical procedure 5 ml of $Ti(OBut)_4$ are introduced in a 50 ml Teflon-lined stainless steel autoclave, together with 1.9 g of TFAA. A small amount of deionizated water (0.4 ml) is added to accelerate the hydrolysis reaction. The system is then heated at 200 °C for 24 h. The obtained white-brown precipitate is washed several times with water and ethanol (96%) and then dried at 105 °C. The washed solid is completely cleaned by irradiation under UV-visible light of a suspension in water for 6 h. As is shown in Fig. 1a, nanoparticles are self-cleaned under UV-visible light, yielding a white solid after the treatment. This cleaning treatment was chosen because it avoids the use of high temperatures or chemicals which can modify the morphology and/or properties of the obtained Ti-TFAA particles.

Characterization methods

A comprehensive examination of the obtained Ti-TFAA powders was conducted using a broad set of characterization techniques and the most relevant features were compared with several commercial TiO_2-based photocatalysts the principal properties of which are depicted in Table 1.

The analyses of the crystalline structure and phase identification were performed by X-ray diffraction (XRD Bruker D8 ADVANCE) with a monochromatized source of Cu-K_a1 radiation (λ ¼ 1.5406 nm) at 1.6 kW (40 KV, 40 mA); samples were prepared by placing a drop of a concentrated ethanol dispersion of particles onto a single crystal silicon plate. High-resolution transmission electron microscopy (HRTEM) images and EDX analyses were obtained on a JEOL 2100F transmission electron microscope (TEM/STEM) operating at 200 kV and equipped with a field emission electron gun providing a point resolution of 0.19 nm; samples were prepared by placing a drop of a dilute ethanol dispersion of nanoparticles onto a 300 mesh carbon-coated copper grid and evaporating immediately at 60 °C.

X-ray photoelectron spectroscopy (XPS) was used to characterize the chemical composition of the samples. XPS spectra were acquired in an ultrahigh vacuum (UHV) chamber with a base pressure of 1 x 10^{-9} mbar using a hemispherical electron energy analyzer (SPECS Phoibos 150 spectrometer) and a monochromatic AlK_a X-ray source (1486.74 eV). XPS spectra

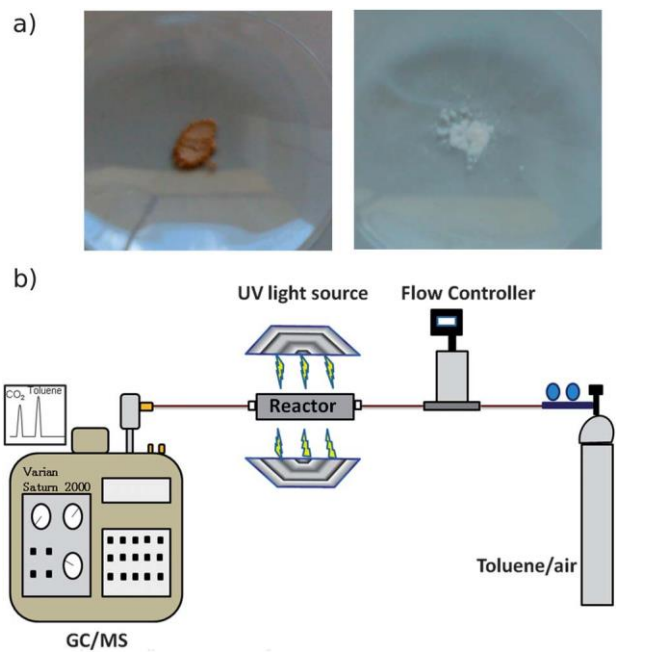

Fig. 1 (a) Ti-TFAA synthesized powder before and after cleaning under UV-visible light irradiation. (b) The experimental setup for testing the photocatalytic activity.

Table 1 Principal characteristics of the Ti-TFAA powder and different commer- cial photocatalysts used in this study

Sample	Anatase : rutile ratio	Crystallite size [±5 nm]	SBET [±10 $m^2 g^{-1}$]
Ti-TFAA	100 : 0	15	111
Degussa P25 (Evonik)	75 : 25	20	49
Evonik P90	86 : 14	15	90
Millenium PC100	100 : 0	15	90

were recorded at the normal emission take-off angle, using an energy step of 0.05 eV and a pass-energy of 10 eV for high resolution data, which provides an overall instrumental peak broadening of 0.4 eV.[32] Carbon and hydroxyl (OH) species were also detected as surface contaminants and the signal from adventitious carbon at 284.6 eV was used for energy calibration. Data processing was performed using CasaXPS software.

Isotherms for adsorption–desorption of N_2 at 77 K were measured using a Micromeritics TriStar 3000 model; the BET areas (SBET) were determined using the Brunauer, Emmett and Teller equation. The infrared spectra of the samples were obtained on Fourier transform infrared spectrometer Thermo Nicolet 6700 FTIR equipment by using the Attenuated Total Re ectance (ATR) method (polyethylene detector). The obtained spectra were averaged from a minimum of 512 scans. On the other hand samples were characterized by means of Raman spectroscopy using a Renishaw inVia spectrometer at 785 and 514 nm laser excitation wavelengths; the measurements were obtained from the average of 10 scans over a range of 100–900 cm^{-1} and using monolithic Si as the calibration source.

The interaction of ammonia with TiO_2 nanoparticles was analyzed with a Nicolet IS10 spectrometer, and the corresponding FT-IR spectra were recorded. Packed reactors were used for the impregnation of the catalysts (100 mg). A flow of 20 ml min^{-1} of the ammonia–argon (65/35) mixture was held for 1 hour. Afterwards, the sample was placed between two CaF_2 windows for its FT-IR analysis.

Testing of the photocatalytic activity

UV-Vis measurements were made with a Perkin Elmer Lambda 950 UV/Vis spectrometer. The same instrument was used for the measurement of the absorption spectrum of TiO_2 nanoparticles. The band gap value was calculated from the Tauc plot[33] ($(ahn)^{1/2}$ *vs.* hn) by extrapolating the linear region to zero. The absorption coefficient (a) was obtained from the experi- mental reflectance data by the Kubelka–Munk algorithm. Finally we represented the $ahn = A(hn - E_g)^2$, $(ahn)^{1/2}$ *vs.* hn plot.

The photocatalytic properties of the synthesized TiO_2 nanoparticles were studied evaluating the oxidation of toluene, a characteristic air pollutant. For all the experiments an annular photoreactor constructed using a Pyrex glass tube was used. The reactor is 140 mm long, with an outer tube diameter of 32 mm and an inner tube diameter of 20 mm to render a total volume of the reactor $V = 0.485$ dm^3. The inner tube was coated with the powder samples by dip-coating, using ethanol as a dispersant agent. Five dip-coating cycles were necessary to deposit 2 mg of each catalyst. Afterwards, the lms were dried at 100 °C for 2 hours. Illumination of the reactor was provided by eight 15 W fluorescent black-light blue-lamps which efficiently emitted UVA light at 315–400 nm, with the maximum wavelength at 365 nm (Philips Cleo®). The UV lamps were placed above and below the reactor. The reaction gas mixture flew between the reactor's inner and outer tubes. The toluene concentration was 18 mg l^{-1} in air and the inlet gas flow rate was 10 ml min^{-1}. Before switching on the UVA light, the catalyst lms were exposed to the gas stream until dark-adsorption equilibrium was reached. On-line detection and quanti cation of toluene, CO_2 and intermediates were performed by GC-MS (Varian Saturn 2000). Fig. 1b shows the experimental setup used for this experiment.

Results and discussion

The crystallinity of the as-prepared powders was examined by X-ray diffraction. As inferred from the pattern depicted in Fig. 2, the sample is crystalline and anatase TiO_2 is the only obtained phase (JCPDS File no. 21-1272). Fig. 3 presents TEM images of the synthesized sample, showing monodispersed well-faceted TiO_2 nanocrystals with truncated rhombic-shape morphology and sizes between 15 and 20 nm. Depending on the truncation grade and the direction from which the crystals are observed, square, hexagonal, and truncated bi-pyramidal shapes can be appreciated (Fig. 3a and b). The high magni cation TEM image (Fig. 4) shows a single nanoparticle. Observed along the [111] zone axis, the image shows the lattice fringes, which are parallel to the edges of the nanocrystalline TiO_2. The interplanar crystal spacing is 0.353 nm, which can be assigned to the lattice spacing of adjacent (101) and (011) crystal planes of anatase TiO_2.[26] The interfacial angle of 82.3° is quite consistent with the theoretical value.[34] The inset in Fig. 4 shows the corresponding

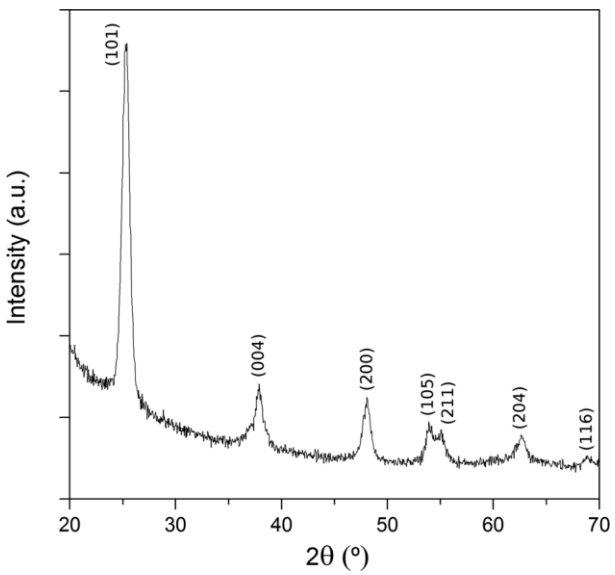

Fig. 2 X-ray diffraction pattern for the synthesized Ti-TFAA powder. All peaks corresponding to the anatase TiO_2 phase.

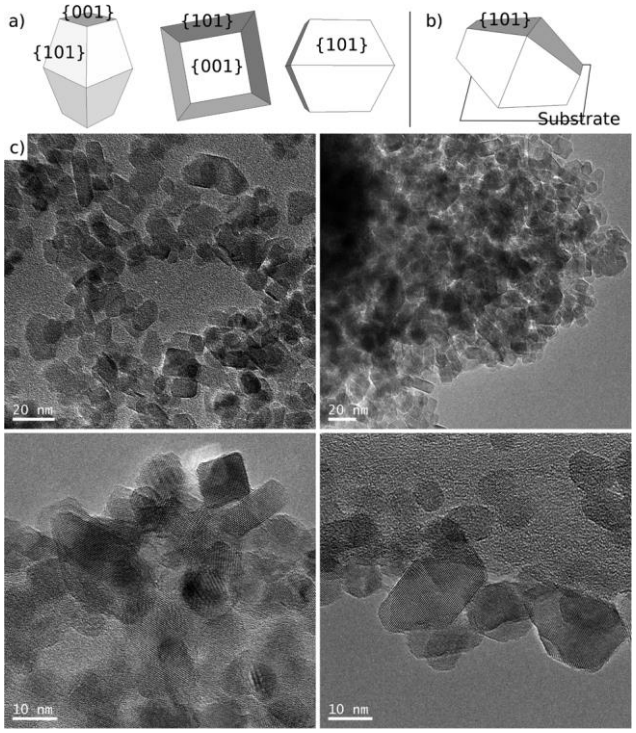

Fig. 3 (a) Schematic representation of anatase crystals with different truncation grades as observed from different directions. (b) Schematic representation of the most entropic orientation for the anatase crystals. (c) TEM images of anatase nanoparticles Ti-TFAA with different orientations.

structural model of the free-standing single crystal. This growth habit must be attributed to the presence of the fluorinated compound; as mentioned in the Introduction section, the use of surface adsorbed fluorine atoms stabilizes the ultra-reactive (001) surface, leading to the formation of capped octahedra of TiO_2 with a certain percentage of {001} facets (Fig. 3a).[14,24] Such an increment in the percentage of {001} facets is not appreciated in the XRD peak area ratios corresponding to the {101} and {004} facets; this must be attributed to the way the samples are prepared for the XRD measurements, which favors the orientation of the nanoparticles with the {101} facets parallel to the substrate, the most entropic orientation (Fig. 3b). The yield of faceted particles is above 90%, as estimated from TEM images using an image analyzer program (Leyca).

In order to check if TFAA releases F^- ions during the semi-solvothermal process, a concentrated solution of $Ca(CH_3COO)_2$ was added to the mother liquor.[35,36] The subsequent precipitation of CaF_2 confirms the partial decomposition of TFAA, so initially we can assume the presence of free fluorine anions in the solution acting as additional capping agents. Next, to verify which species have been adsorbed onto the surface of the anatase nanoparticles, high-resolution XPS measurements were carried out. In particular the F1s, Ti2p and C1s core levels were evaluated. Fig. 5a first shows the XPS spectrum corresponding to the F1s level and, as observed, two main contributions are readily detected. The smaller contribution at ~684 eV is characteristic of fluorinated TiO_2 systems and can be ascribed to an F–Ti–O chemical environment,[24,26,37–39] *i.e.*, it is indicative of the presence of Ti–F species at the crystal surface. On the other hand the main contribution at ~688 eV can be attributed to C–F species,[24,26,27,37–39] which in our case are likely to come from $–CF_3$ groups of TFAA adsorbed on the particle surface. Therefore, it can be concluded that fluorine is present on the surface of TiO_2 particles as both surface atoms and $–CF_3$ groups. Fig. 5b then displays the XPS spectrum corresponding to the Ti2p core level of the synthesized sample; for comparison the spectrum of a commercial TiO_2 sample is also depicted in this figure. As observed a chemical shift of 0.27 eV towards higher binding energy is detected for the Ti-TFAA composition. A similar shifting value has been previously reported for similar systems,[24,26,37,40] but apart from this variation in binding energy, the two XPS spectra in Fig. 5b are almost identical if shifted for overlapping. Hence we can presume that the presence of

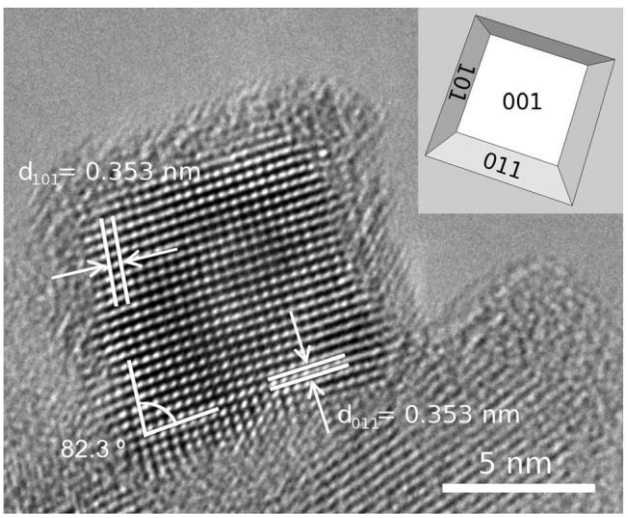

Fig. 4 High magnification TEM image of one TiO_2 anatase nanocrystal. The inset shows the schematic representation as viewed from the [111] direction.

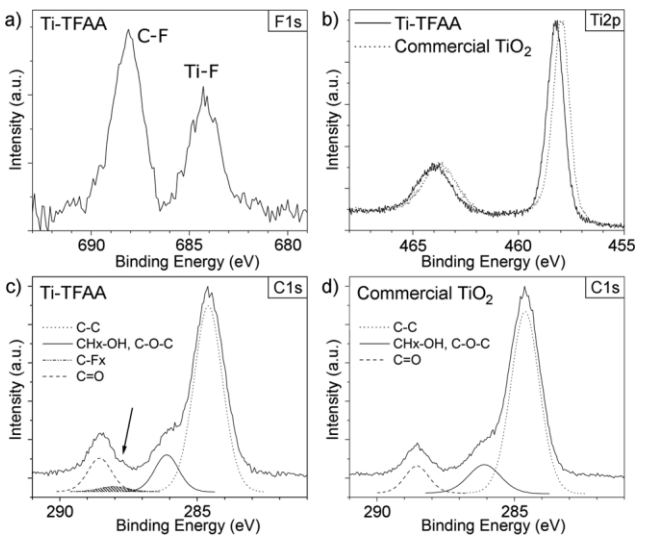

Fig. 5 High-resolution XPS spectra corresponding to: (a) F1s region for the Ti- TFAA sample, (b) Ti2p region for the Ti-TFAA and commercial P25 samples, (c) C1s region for the Ti-TFAA sample, and (d) C1s region for the commercial P25.

fluorine does not produce significant changes in the inner structure of TiO_2 nanograins, which is to say that the Ti^{4+} oxidation state of bulk TiO_2 remains unaltered and the incorporation of F atoms into the TiO_2 lattice can be ruled out. Finally, Fig. 5c and d show the C1s spectral decomposition corresponding to Ti-TFAA and commercial TiO_2 samples, respectively. In both cases C–C, C–O, and C]O convoluted components can be observed (in commercial TiO_2 these signals come from the carbonated surface; in the Ti-TFAA samples they arise from both the carbonates and the TFAA groups). But as observed there is one additional signal in the Ti-TFAA system, a weak shoulder located at a binding energy slightly below that of the C=O (arrow marked in Fig. 5c). This signal might be associated with the existence of C–F_x sites, which have previ- ously been assigned by some authors to low coordinated states in fluorinated TiO_2 surfaces.[39,41–43] However, the truth is that the existence of this additional component cannot be determined just by leaning on the inspection and fitting procedure of the C1s photoemission signal. In order to have more consistent evidence, selected Ti-TFAA samples were bombarded with low energy (1 keV) Ar ions and the XPS measurements were repeated. This sputtering process removes not only adventitious carbon and adsorbed water but also some other molecules at the surface of the particles, so it can be useful for discerning the origin of chemically shifted components present in the C1s core level signal. As shown in Fig. 6a upon normalization of C1s spectra, after being irradiated, the high binding energy peak (on the left) undergoes a decrease in intensity and a change in line shape which somehow blur the shoulder ascribed to the C–F_x component, so this indirectly confirms the presence of the –CF_3 related groups adsorbed on the TiO_2 surface. But moreover, the F1s raw photoemission signal of the irradiated sample was also recorded and displayed together with that of the as-prepared sample (Fig. 6b). Two interesting results were observed: first, as happened to the C–F_x component of the C1s core level, the signal ascribed to the presence of C–F species also experiences a drastic decrease in intensity after being bombarded. Second, the component related to the Ti–F species remains unaltered after the irradiation. This last feature actually stands for a form bonding strength between the F atoms and the TiO_2 nanoparticles, highly favorable for an enhanced photoactivity.

Following the XPS analyses, FT-IR spectra of the modified TiO_2 nanocrystals were recorded to verify whether TFAA molecules are indeed adsorbed on the surface of the nanoparticles.

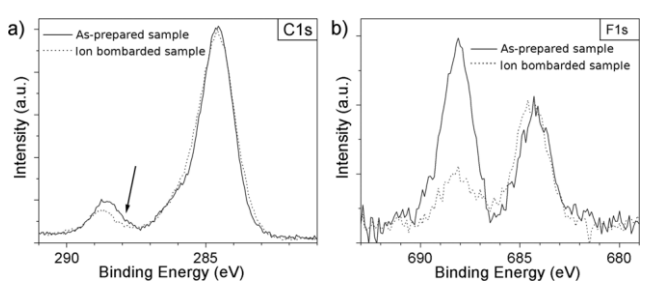

Fig. 6 High-resolution XPS spectra of the Ti-TFAA powder before and after bombarding with low energy (1 keV) Ar ions. (a) C1s region and (b) F1s region.

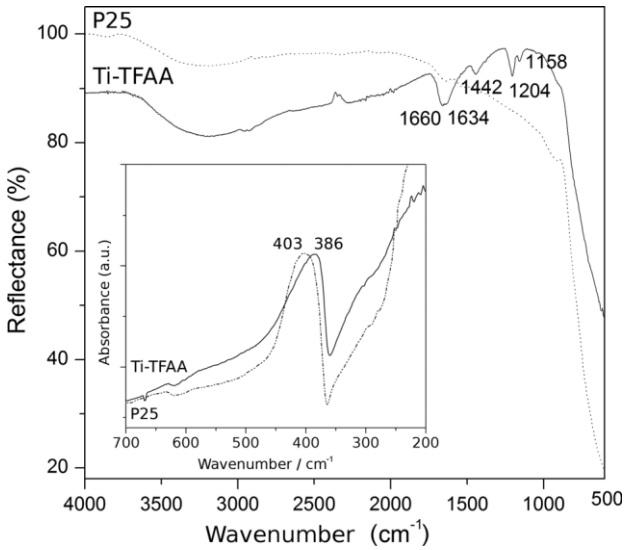

Fig. 7 IR-ATR spectra of the Ti-TFAA and commercial P25 samples. The inset highlights the Ti–O stretching region for both spectra.

For comparison the commercial Degussa P25 TiO_2 powder was analyzed by FT-IR as well, and as depicted in Fig. 7 significant differences can be observed between the spectra of both materials. First, the bands at 1634 and 1442 cm^{-1} are only observed in the Ti-TFAA sample, and can be assigned to the asymmetric and symmetric C]O stretching vibrations of TFAA, respectively.[44] In a similar way the bands observed at 1204 and 1158 cm^{-1} correspond to the C–F stretching vibration,[25] and are missing in the spectra of the commercial sample. A more in-depth analysis of the low wavenumber region (200 to 700 cm^{-1}, see the inset in Fig. 7) reveals the presence of one absorption band at 386 cm^{-1} for the Ti-TFAA composition. This band shall be assigned to the Ti–O vibration, although when compared to commercial P25 its position is shifted to lower wavenumbers (centered at 403 cm^{-1} for the commercial sample). Such shifting can only be attributed to the adsorption of TFAA on the surface of TiO_2 crystals; as it has been reported when a carboxylic group bonds to an electron-deficient atom such as Ti^{4+}, its IR absorption bands shift to lower wavenumbers.[45] Apart from that, we can also use the difference between the carboxylate stretching frequencies, $D = n_{as} - n_{sym}$, to further identify the coordination mode of the carboxylic group.[46,47] Generally, monodentate complexes exhibit D values much larger than those of the corresponding ionic structures; in contrast bidentate chelating complexes exhibit D values significantly smaller than the ionic values, whereas bridging complexes have values less than, but close to, the ionic value, see Scheme 1.[27] In our case the experimental D value for the Ti-TFAA samples is 1634 - 1442 = 192 cm^{-1}, *i.e.* smaller than that for isolated hydrogen-bonded dimers (345 cm^{-1}),[27] so consequently TFAA species are mainly bonded to the Ti atoms in a bidentate mode (bridging or chelating), although the existence of other minority coordination modes should not be completely neglected. Again this is an excellent scenario for our purposes, since a bidentate coordination mode through the oxygen atoms

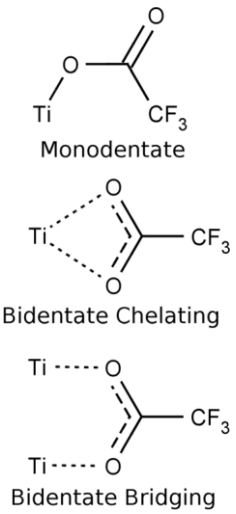

Scheme 1 Possible coordination modes of a TFAA molecule.

of the carboxylic group is known to contribute to stabilization of the TiO_2 {001} facets.[20]

Fig. 8 shows the Raman spectra obtained for both the Ti-TFAA nanocrystals and the commercial P25 sample. As previously reported for other fluorine-terminated TiO_2 compounds,[37] two main features can be observed for the Ti-TFAA composition: the shi□ing of the E_g mode to higher frequencies and the weakening in intensity of the B_{1g} mode. As suggested by Pan and coworkers,[37] these changes in the surface structure are imposed by the presence of surface Ti–F bonds, so consequently this technique also con□rms the presence of fluorine atoms adsorbed on the surface of Ti-TFAA particles.

Finally the adsorption of ammonia on the Ti-TFAA nanoparticles was analyzed, and in this case the comparison was established not with Degussa P25 but with P90 and PC100 commercial catalysts because these two powders show a speci□c surface which is more similar to that of our Ti-TFAA composition (see Table 1). This interaction with the NH_3 molecule has been widely used as a powerful tool to determine the proportion and properties of Lewis and Br¨onsted centres at the catalyst surface.[48,49] Lewis acid centers are characterized by bands present between 1215 and 1000 cm^{-1}. The greater the wavenumber of these bands, the higher the acidic character of these centers, so typically bands can be found between 1215 and 1180 cm^{-1} that correspond to strong Lewis acid centers (SLACs), whereas weak Lewis acid or physisorption centers (WLACs) show bands between 1150 and 1000 cm^{-1}. Likewise, Br¨onsted acid centers (BAC) are characterized by a band centered at 1460–1430 cm^{-1}. Finally the NH_3 interaction can also occur simultaneously at strong Lewis acid and basic centers; this leads the molecule to break and bands between 1340 and 1320 cm^{-1} are then observed.[50,51] Bearing this in mind, Fig. 9 shows the FT-IR spectra for the NH_3 interaction of P90, PC100 and Ti-TFAA samples. As observed all these three TiO_2-based catalysts evidence the presence of both Lewis and Br¨onsted acid centers. Also PC100 and Ti-TFAA samples, both containing 100% of

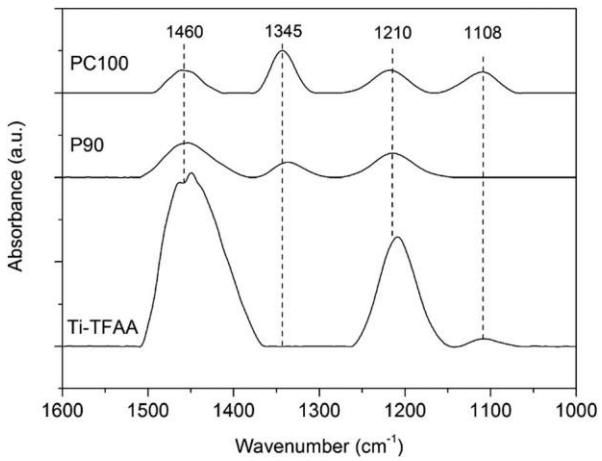

Fig. 9 FT-IR spectra of the Ti-TFAA, P90 and PC100 powders.

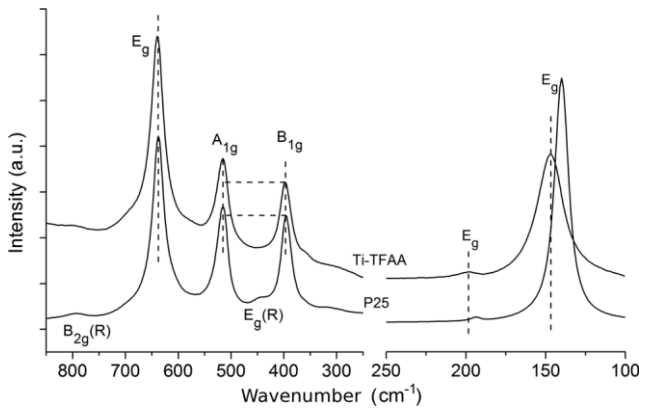

Fig. 8 Raman spectra for the Ti-TFAA and P25 samples. Bands corresponding to the rutile phase in P25 are denoted as (R).

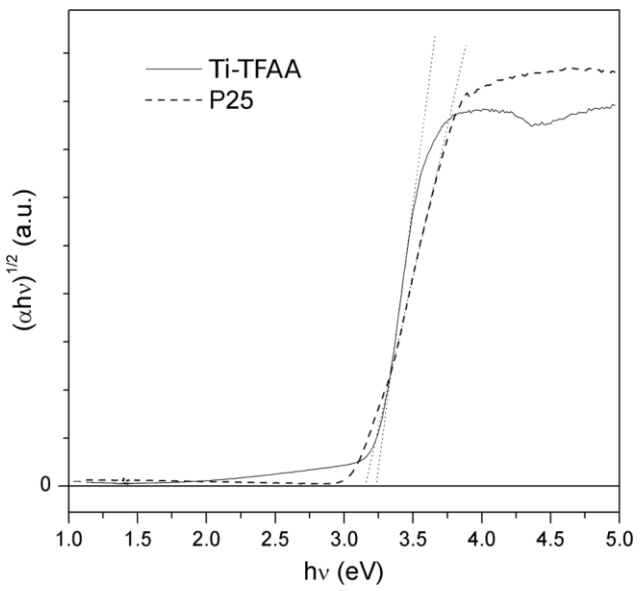

Fig. 10 Tauc plot from the UV-vis absorption spectra corresponding to the Ti-TFAA and P25 samples.

anatase, show the existence of weak Lewis centers on their surface (band around 1110 cm^{-1}). However whereas the two commercial powders also show the dissociation of ammonia at strong Lewis acid and basic centers, with a band around 1340 cm^{-1}, no such band is observed for the Ti-TFAA sample. This lack of basic reactivity towards NH_3 again suggests a different surface structure for the TiO_2-modified nanoparticles; although more in-depth analyses are required (currently in progress), the occurrence of adsorbed fluorine species at the strong Lewis acid Ti^{5c4+} centers and a weaker basicity of the surface anions (O_2^{2-}) may explain the absence of dissociative centers in the Ti-TFAA powder.

Photocatalytic response

Different experiments were conducted to evaluate the photocatalytic response of the Ti-TFAA nanoparticles synthesized here. First, the UV-vis diffuse reflectance spectrum of the compound was measured and the band gap was calculated from the Tauc $((ah\nu)^{1/2}$ *vs.* $h\nu)$ plot.[33] As shown in Fig. 10 the absorption edge is slightly shifted with respect to Degussa P25 and yields a band gap value of 3.20 eV, the expected value for TiO_2 anatase. P25 photocatalyst presents a lower value because it is a 75 : 25 mixture of anatase (3.16 eV) and rutile (3.02 eV), respectively. The presence of an additional shoulder in the visible region (2.0 to 3.25 eV) is due to the presence of TFAA adsorbed on the surface of the nanocrystals.

Followed by this, the photocatalytic performance of the Ti-TFAA sample was evaluated by degradation of gaseous toluene under UV illumination as described in the Experimental section (see also Fig. 1). Fig. 11a first shows the evolution of the toluene concentration *versus* the reaction time and clearly evidences a better photocatalytic activity for the Ti-TFAA sample; after 20 minutes the total inlet concentration of toluene is removed and this situation remains unaltered for the whole experiment. In contrast, the photodegradation attained by the commercial catalysts also reaches a maximum after 20 minutes but then they get gradually deactivated and after 180 minutes only a degradation of 30 to 40% of the toluene inlet can be achieved with the P90 and PC100 powders. Fig. 11b then shows the evolution of CO_2 in the outlet stream from the reactor. As observed the sequence in toluene mineralization follows the

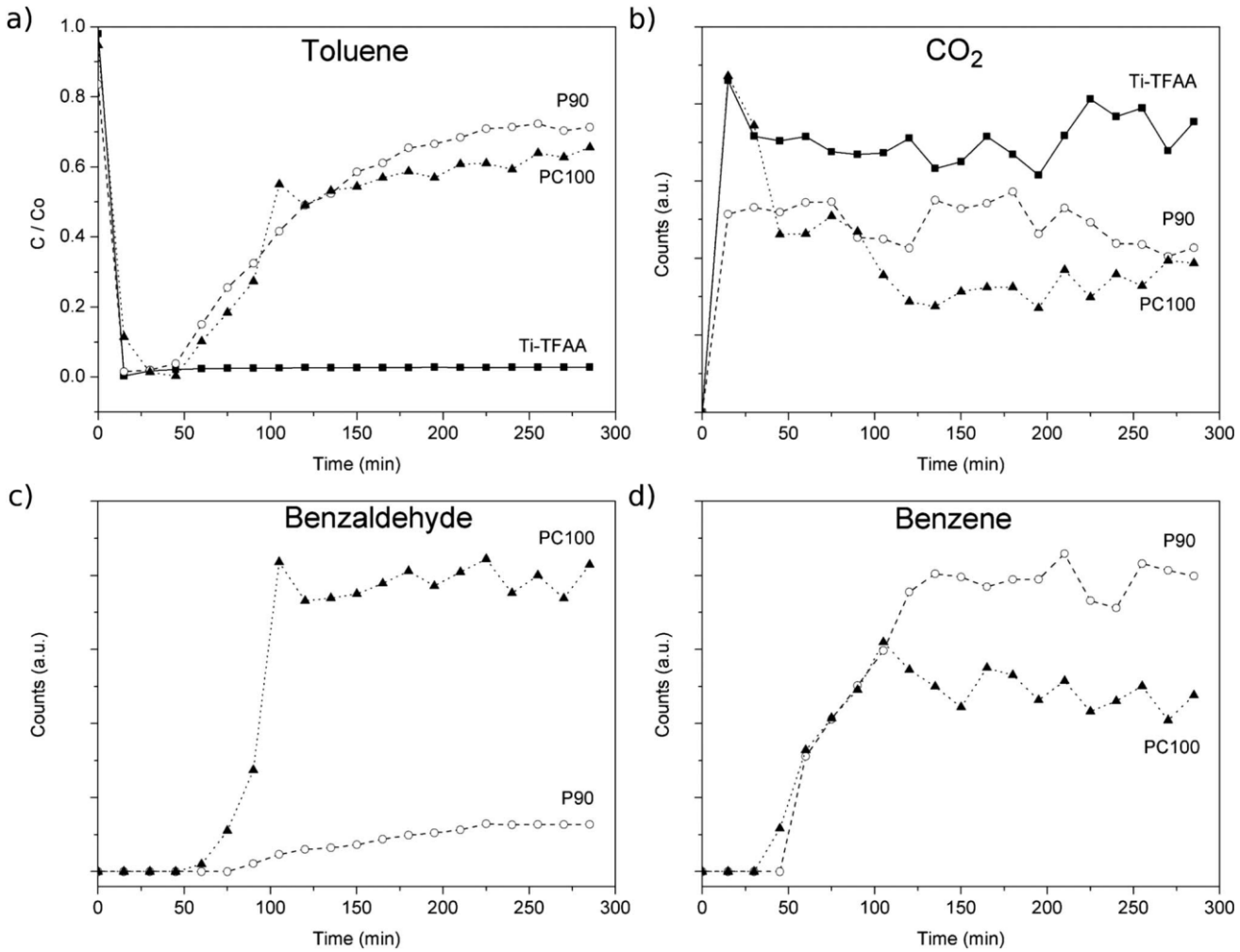

Fig. 11 Evolution with the reaction time of: (a) toluene concentration, (b) CO_2 concentration, (c) benzaldehyde concentration and (d) benzene concentration for the Ti-TFAA, P90 and PC100 photocatalysts.

same order of the photodegradation and the highest production of CO_2 is achieved by the Ti-TFAA sample. These results should be interpreted taking into consideration that during the photocatalytic process the semiconductor photocatalyst can deactivate, especially when dealing with oxidizing aromatics.[52,53] In particular according to d'Hennezel *et al.*,[54] the primary pathway in the photocatalytic oxidation (PCO) of toluene is the hydrogen abstraction from the methyl group by direct transfer of h^+ or_OH radicals, leading to a benzyl radical. The benzyl radical further transforms into three initial by-products, namely benzaldehyde, benzoic acid, and benzyl alcohol.[55] Benzene is subsequently generated from decomposition of benzoic acid *via* a photoKolbe mechanism,[56] and then all these intermediates can be involved in ring opening reactions triggered by h^+ and _OH species. Further bond breakage finally produces various compounds with smaller molecular weights such as acetic acid, methanol, formic acid, formaldehyde and, eventually, CO_2 and H_2O. So in this sense, if the mineralization of toluene does not easily proceed to the end, partially oxidized intermediates would settle in the semiconductor photocatalyst, exerting poisoning effects on its surface and finally leading to its deactivation. Going back to our experiments, Fig. 11c and d show the evolution of benzaldehyde and benzene species as a function of the reaction time. Whereas both compounds can be detected at the reactor outlet when commercial P90 and PC100 are used as photocatalysts (the accumulation profiles matching the deactivation trends in Fig. 11a), none of these by-products were found when the Ti-TFAA powder was used. Ti-TFAA allows faster surface regeneration, and therefore less deactivation. In contrast PC100 and P90 have slower surface regeneration, so the surfaces are eventually saturated and the reaction reaches a steady state. In other words, the Ti-TFAA powder successfully transforms toluene and the harmful intermediates into less toxic compounds. Obviously this must be attributed to the specific characteristics of the TiO_2 nanoparticles that we have succeeded to prepare here. First, the Ti-TFAA particles show a stabilization of {001} facets, which not only display a higher reactivity, but also contribute to decrease the recombination processes between the electron–hole pair, facilitating the migration of electrons to the surface.[57–62] Second, the electron withdrawing role of both the $–CF_3$ groups and the F^- ions also reduces the recombination rate of photogenerated electrons and holes of TiO_2.[24] And finally, the surface area of the nanosized Ti-TFAA catalyst, 111.25 $m^2\ g^{-1}$ (clearly larger than that of P25, 49.16 $m^2\ g^{-1}$), is also propitious for photon harvesting, absorption of guest species, and for the photoinduced charge separation.[63] All in all these features yield a highly photocatalytic material.

Finally, in addition to the improved UV-visible light activity, the Ti-TFAA nanoparticles also show strong stability and durability for the decomposition of toluene. Fig. 12 shows the photoactivity of the Ti-TFAA film in toluene photodegradation after three consecutive cycles. The surface of the film was exposed to a stream of air and UVA light for 30 minutes after each cycle in order to degrade the adsorbed molecules prior to a new experiment. As can be observed the stability of the material and the reproducibility of the photodegradation results are maintained at least for the three cycles of photodegradation, suggesting that

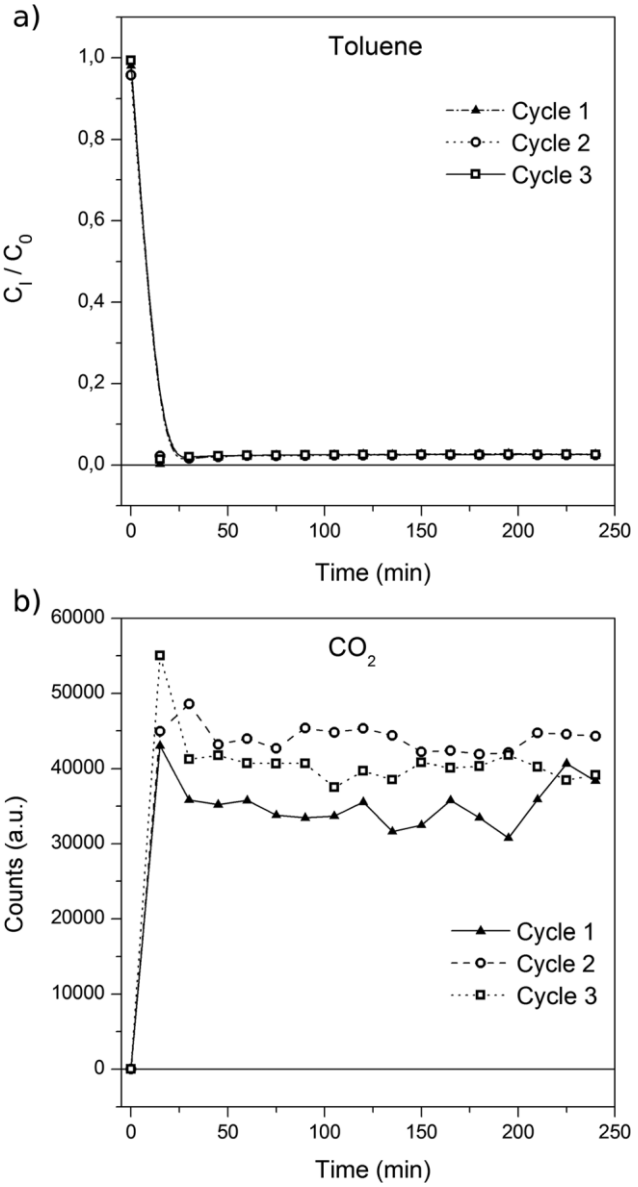

Fig. 12 Recycling test of toluene photodegradation: evolution with the time of (a) toluene concentration and (b) CO_2 concentration.

this material has remarkable potential for practical applications. During these cycles the stability of TFAA adsorbed on the surface was checked by FT-IR spectroscopy, and the experimental data indicate that TFAA is oxidized and gradually decomposes during the photodegradation tests under the UV radiation (see ESI†), probably leaving fluorine ions adsorbed on the surface that prevents the decay of the photocatalytic performance by losing the $–CF_3$ groups.

Conclusions

Well-faceted TiO_2 anatase nanocrystals with capped octahedron morphology have been obtained through a facile one step semi-solvothermal reaction, in which trifluoroacetic acid (TFAA) is used as an electron scavenger and morphological control agent.

As evidenced through a broad spectrum of characterization techniques, trifluoroacetic acid adsorbs on the surface of TiO_2 nanoparticles either through the oxygen atoms of the TFAA molecule itself or as F^- ions (released from the partial decomposition of TFAA), thereby stabilizing the highly photoactive {001} facets of anatase. This added to the electron withdrawing role of both the $–CF_3$ groups and F^- ions, eventually leading to an enhanced photocatalytic performance; compared to commercial photocatalysts, the TFAA modified TiO_2 nanoparticles prepared here increase the mineralization of pollutant toluene, and more important even, by impeding the accumulation of intermediate species these Ti-TFAA particles do not get deactivated during the whole photodegradation process.

Acknowledgements

This work was supported by the Spanish Ministry of Economy and Competitiveness (MINECO) through the projects IPT-120000-2010-033 (GESHTOS), IPT-2011-1113-310000 (NANOBAC), CICYTMAT 2010-16614, MAT2010-18432 and CSD2008-00023. Dr T. Jardiel also acknowledges the JAE-Doc contract of the Spanish National Research Council (CSIC) and the European Science Foundation (ESF). Dr M. Peiteado acknowledges the Ramon y Cajal Program of MINECO for the financial support.

Notes and references

1 L. I. Halaoui, N. M. Abrams and T. E. Mallouk, *J. Phys. Chem. B*, 2005, 109, 6334–6342.
2 X. S. Peng, J. P. Wang, D. F. Thomas and A. C. Chen, *Nanotechnology*, 2005, 16, 2389–2395.
3 M. Tian, G. Wu, B. Adams, J. Wen and A. Chen, *J. Phys. Chem. C*, 2008, 112, 825–831.
4 P. S. Liu, W. P. Cai, M. Fang, Z. G. Li, H. B. Zeng, J. L. Hu, X. D. Luo and W. P. Jin, *Nanotechnology*, 2009, 20, 285707. 5 A. Di Paola, G. Marci, L. Palmisano, M. Schiavello, K. Uo-saki, S. Ikeda and B. Ohtani, *J. Phys. Chem. B*, 2002, 106, 637–645. 6 U. Stafford, K. A. Gray, P. V. Kamat and A. Varma, *Chem. Phys. Lett.*, 1993, 205, 55–61.
7 G. Riedel and J. R. Bolton, *J. Phys. Chem.*, 1995, 99, 4215–4224.
8 K. Tanaka, M. F. V. Capule and T. Hisanaga, *Chem. Phys. Lett.*, 1991, 187, 73–76.
9 T. Ohno, K. Sarukawa and M. Matsumura, *J. Phys. Chem. B*, 2001, 105, 2417–2420.
10 T. Ohno, K. Sarukawa and M. Matsumura, *New J. Chem.*, 2002, 26, 1167–1170.
11 O. O. Prieto-Mahaney, N. Murakami and B. Ohtani, *Chem. Lett.*, 2009, 38, 238–239.
12 O. Carp, C. L. Huisman and A. Rell, *Prog. Solid State Chem.*, 2004, 32, 33–177.
13 A. Sclafani and J. M. Hermann, *J. Phys. Chem.*, 1996, 100, 13655–13661.
14 C. Z. Wen, H. B. Jiang, S. Z. Qiao, H. G. Yang and G. Q. (Max) Lu, *J. Mater. Chem.*, 2011, 21, 7052–7061.
15 L. Ye, J. Mao, J. Liu, Z. Jiang, T. Peng and L. Zan, *J. Mater. Chem. A*, 2013, 1, 10532–10537.
16 B. Wu, C. Guo, N. Zheng, Z. Xie and G. D. Stucky, *J. Am. Chem. Soc.*, 2008, 17563–17567.
17 Y. Luan, L. Jing, Y. Xie, X. Sun, Y. Feng and H. Fu, *ACS Catal.*, 2013, 3, 1378–1385.
18 S. Selçuk and A. Selloni, *J. Phys. Chem. C*, 2013, 117, 6358–6362.
19 T. Jardiel, D. G. Calatayud, M. Rodríguez, M. Peiteado, D. Fernández-Hevia and A. C. Caballero, *J. Alloys Compd.*, 2013, 551, 481–484.
20 D. G. Calatayud, T. Jardiel, M. Rodríguez, M. Peiteado, D. Fernández-Hevia and A. C. Caballero, *Ceram. Int.*, 2013, 39, 1195–1202.
21 K. L. Lv and Y. M. Xu, *J. Phys. Chem. B*, 2006, 110, 6204–6212.
22 V. Maurino, C. Minero, G. Mariella and E. Pelizzetti, *Chem. Commun.*, 2005, 2627–2629.
23 Y. Xu, K. Lv, Z. Xiong, W. Leng, W. Du, D. Liu and X. Xue, *J. Phys. Chem. C*, 2007, 111, 19024–19032.
24 H. G. Yang, C. H. Sun, S. Z. Qiao, J. Zou, G. Liu, S. C. Smith, H. M. Cheng and G. Q. Lu, *Nature*, 2008, 453, 638–641.
25 J. C. Yu, W. Ho, J. Yu, S. K. Hark and K. Iu, *Langmuir*, 2003, 19, 3889–3896.
26 X. H. Yang, Z. Li, C. Sun, H. G. Yang and C. Li, *Chem. Mater.*, 2011, 23, 3486–3494.
27 X. Meng, L. Qi, Z. Xiao, S. Gong, Q. Wei, Y. Liu, M. Yang and F. Wang, *J. Nanopart. Res.*, 2012, 14, 1176.
28 S. C. Padmanabhan, S. C. Pillai, J. Colreavy, S. Balakrishnan, D. E. McCormack, T. S. Perova, Y. Gu'ko, S. J. Hinder and J. M. Kelly, *Chem. Mater.*, 2007, 19, 4474–4481.
29 K. Lv, B. Cheng, J. Yu and G. Liu, *PCCP Phys. Chem. Chem. Phys.*, 2012, 14, 5349–5362.
30 N. V. Golubko, M. I. Yanovskaya, I. P. Romm and A. N. Ozerin, *J. Sol-Gel Sci. Technol.*, 2001, 20, 245–262.
31 B. E. Yoldas, *J. Mater. Sci.*, 1986, 21, 1087–1092.
32 R. Gago, A. Redondo-Cubero, M. Vinnichenko, J. Lehmann, F. Munnik and F. J. Palomares, *Mater. Chem. Phys.*, 2012, 136, 729–736.
33 J. Tauc, R. Grigorovici and A. Vancu, *Phys. Status Solidi B*, 1966, 15, 627–637.
34 J. Zhu, S. Wang, Z. Bian, S. Xie, C. Cai, J. Wang, H. G. Yang and H. X. Li, *CrystEngComm*, 2010, 12, 2219–2224.
35 J. Yu and L. Shi, *J. Mol. Catal. A: Chem.*, 2010, 326, 8–14.
36 D. O'Hagan, *Chem. Soc. Rev.*, 2008, 37, 308–319.
37 J. Pan, G. Liu, G. Q. M. Lu and H.-M. Cheng, *Angew. Chem., Int. Ed.*, 2011, 50, 2133–2137.
38 M. Senna, V. Sepelak, J. Shi, B. Bauer, A. Feldhoff, V. Laporte and K. D. Becker, *J. Solid State Chem.*, 2012, 187, 51–57.
39 C. Ni, Z. Zhang, M. Wells, T. P. Beebe Jr, L. Pirolli, L. P. Méndez De Leo and A. V. Teplyakov, *Thin Solid Films*, 2007, 515, 3030–3039.

40 G. Liu, H. G. Yang, X. Wang, L. Cheng, H. Lu, L. Wang, G. Qing, M. Lu and H. Cheng, *J. Phys. Chem. C*, 2009, 21784–21788.
41 K. Ford, B. J. Battersby, B. J. Wooda and I. R. Gentle, *J. Colloid Interface Sci.*, 2012, 370, 162–169.
42 K. K. Ho, A. F. Lee and A. Bismarck, *Carbon*, 2007, 45, 775–784.
43 X. Cuia, S. Zhongb, J. Yana, C. Wanga, H. Zhanga and H. Wanga, *Colloids Surf., A*, 2010, 360, 41–46.
44 L.-F. Liao, C.-F. Lien and J.-L. Lin, *Phys. Chem. Chem. Phys.*, 2001, 3, 3831–3837.
45 S. W. Boettcher, M. H. Bartl, J. G. Hu and G. D. Stucky, *J. Am. Chem. Soc.*, 2005, 127, 9721–9730.
46 G. Deacon and R. Phillips, *Coord. Chem. Rev.*, 2005, 33, 227–
250.
47 M. Nara, H. Torii and M. Tasumi, *J. Phys. Chem.*, 1996, 100, 19812–19817.
48 B. Bonelli, M. Cozzolino, R. Tesser, M. Diserio, M. Piumetti, E. Garrone and E. Santacesaria, *J. Catal.*, 2007, 246, 293–300.
49 J. J. Murcia, M. C. Hidalgo, J. A. Navío, J. Araña and J. M. Doña-Rodríguez, *Appl. Catal., B*, 2013, 142–143, 205–213.
50 K. Hadjiivanov, *Appl. Surf. Sci.*, 1998, 135, 331–338.
51 J. Araña, D. Portillo-Carrizo, J. A. O. Méndez, J. A. H. Melián, J. M. D. Rodríguez, J. Pérez-Peña and O. González Díaz, *J. Photochem. Photobiol., A*, 2012, 249, 61–69.
52 Y. Luo, *J. Catal.*, 1996, 163, 1–11.
53 M. L. Sauer, M. A. Hale and D. F. Ollis, *J. Photochem.*
Photobiol., A, 1995, 88, 169–178.
54 O. d'Hennezel, P. Pichat and D. F. Ollis, *J. Photochem.*
Photobiol., A, 1998, 118, 197–204.
55 T. Guo, Z. Bai, C. Wu and T. Zhu, *Appl. Catal., B*, 2008, 79, 171–178.
56 M. Sleiman, P. Conchon, C. Ferronato and J.-M. Chovelon, *Appl. Catal., B*, 2009, 86, 159–165.
57 X. Wu, Z. Chen, G. Q. M. Lu and L. Wang, *Adv. Funct. Mater.*, 2011, 21, 4167–4172.
58 H. G. Yang, G. Liu, S. Z. Qiao, C. H. Sun, Y. G. Jin, S. C. Smith, J. Zou, H. M. Cheng and G. Q. Lu, *J. Am. Chem. Soc.*, 2009,
131, 4078–4083.
59 X. Han, Q. Kuang, M. Jin, Z. Xie and L. Zheng, *J. Am. Chem. Soc.*, 2009, 131, 3152–3153.
60 F. Amano, O. O. Prieto-Mahaney, Y. Terada, T. Yasumoto, T. Shibayama and B. Ohtani, *Chem. Mater.*, 2009, 21, 2601–2603.
61 G. Liu, C. H. Sun, H. G. Yang, S. C. Smith, L. Z. Wang, G. Q. Lu and H. M. Cheng, *Chem. Commun.*, 2010, 46, 755– 757.
62 Z. Zheng, B. Huang, J. Lu, X. Qin, X. Zhang and Y. Dai, *Chem.–Eur. J.*, 2011, 17, 15032–15038.
63 J. Fu, Y. Tian, B. Chang, F. Xi and X. Dong, *J. Solid State Chem.*, 2013, 199, 280–286.